Article:
Chaurasia, S., Kaur, Channprit, Borisenko, N. G. et al. (3 more authors) (2017) Enhancement of keV X-rays from low-density cellulose triacetate (TAC) foam targets. Physics of Plasmas. 073110. ISSN 1089-7674

https://doi.org/10.1063/1.4991410

Enhancement of keV X-rays from low-density cellulose triacetate (TAC) foam targets

S. Chaurasia[1], Channprit Kaur[1,2], N. G. Borisenko[3], J. Pasley[4], A. Orekhov[3], M. N. Deo[1]

[1]*High Pressure and Synchrotron Radiation Physics Division, Bhabha Atomic Research Centre, Trombay, Mumbai - 400085, India*

[2]*Homi Bhabha National Institute, Anushaktinagar, Mumbai- 400094, India*

[3]*P. N. Lebedev Physics Institute, Leninsky Pr 53, Moscow, Russia.*

[4]*York Plasma Institute, Department of Physics, University of York, York, YO10 5DQ, UK*

*email: pgshivanand@gmail.com, phone No. 91-22-25590205, Fax No. 91-22-25505296

The interaction of a high-power laser with a low-density foam target can in some instances result in a significant enhancement in x-ray generation relative to that when the same laser is incident upon a homogenous solid. In this paper, we present x-ray emission studies from foam targets where the density is varied from under-dense to over-dense. The targets are irradiated with the first harmonic of Nd: Glass laser. The laser intensity on the target was approximately 2 x 10^{14} W/cm^2 with 500 ps pulse duration. Mass-matched cellulose triacetate foam targets with densities of 2 mg/cc, 4 mg/cc, 7 mg/cc and 20 mg/cc were used. The areal density presented by the targets on the laser beam axis was held constant at 0.2 mg/cm^2 by varying the target thickness in inverse proportion to the density. The x-ray yield in the spectral range (5- 8 keV) and (4.5- 16 keV) was found to be enhanced by approximately 2.3 times in foam targets with density 2 mg/cc (under-dense) compared with foam targets of density 20 mg/cc (over-dense).

Key words: Laser coupling, supersonic heat wave, volume plasma heating.

I. INTRODUCTION

Laser-driven multi-keV x-ray sources are powerful tools for radiography and are used in experiments for laboratory astrophysics, high-energy-density physics, and Inertial Confinement Fusion (ICF) research[1]. These experiments often require high laser to x-ray Conversion Efficiency (CE) in order to ensure that the radiographic source is significantly brighter than the self emission of the object being probed at the x-ray energies of interest. Multi-keV x-rays are typically radiated from the high temperature region of the plasma, which is highly ionized. When a high power laser is incident upon a homogenous solid, the x-ray emission region for the dense regions of the target is limited by the fact that the laser cannot penetrate beyond what is known as the critical surface, where the laser frequency equals the electron plasma frequency. For Nd: Glass laser light this density is typically of the order of 4 mg/cc, meaning that the laser is unable to heat the dense regions of the target directly. The denser portions of the target are heated by electron thermal conduction and hydrodynamic processes. At densities approaching solid, temperatures will typically be several orders of magnitude lower than in the coronal plasma in which the laser is able to heat directly. However, if the target material is under-dense, meaning that the ionized electron density is lower than the laser critical density, the laser can penetrate and heat the target directly to a much greater depth. Once the under-dense material is partially ionized by a combination of multi-photon and cascade ionization processes, the rest of the laser energy is predominantly absorbed by saturable inverse bremsstrahlung, creating an ionization wave[2]. If the ionization wave moves forward into the cold material at greater than the sound speed in the already heated matter, then it is said to be supersonic, and significant hydrodynamic motion will not be induced at the location of the heat front, even though the pressure gradients

are very large. Such a heat front can also outrun the rarefaction wave that propagates inward from the free surfaces of the heated plasma, since this wave can only propagate at the local sound speed. The large volume supersonic heating of low-density material with little energy loss in hydrodynamic motion has previously been associated with enhanced x-ray production[3-5]. Thus low-density foams are found to be suitable candidates for the efficient production of laser-generated x-rays[6]. It has previously been shown that the increase in the CE in the lower keV x-ray range in sub-critical foams is less than in the higher keV x-ray spectral range[7]. Given that the most commonly produced foams are quite low-Z, an efficient multi-keV x-ray source has been demonstrated by laser irradiation of Ge & Ti-doped foam targets.[8-9] Enhancement in the soft-x-ray region has also been reported with low-density carbon foam.[10] Furthermore, low-density foam targets, both low Z and high Z, have become a material of interest in a number of different scenarios related to ICF[11-14], laser driven shock studies[15], laser beam smoothing[16], opacity measurement[17], foil acceleration[18], and equation of state studies[19].

In this paper, measurements of x-ray yield in two spectral ranges, 5- 8 keV and 4.5-16 keV are reported from foam targets where the ionized density is varied from under-dense to over-dense. This enables experimental verification of the utility of using targets of a particular density relative to critical density, as x-ray sources both in laboratory applications and elsewhere. The targets are irradiated with the first harmonic of a Nd: Glass laser. Hydrodynamic expansion of the target is diagnosed using two-frame optical shadowgraphy.

II. EXPERIMENTAL DETAILS

The laser system used in these experiments is a Nd: Glass silicate laser system at Bhabha Atomic Research Centre (BARC). In this experiment the energy on target is approximately 7.5 J in a 500

ps Gaussian pulse for a laser wavelength of 1062 nm. The laser is focused with an f/5 lens into a chamber evacuated to $4x10^{-5}$ mbar. The focal spot diameter at the target front-surface is 100μm (Gaussian spatial profile) thereby giving a peak intensity of ~ 2 x 10^{14} W/cm^2 on target. Schematic of the set up is shown in Fig. 1a.

The polymer foam structure such as open pores, semi-closed pores and closed pores can be achieved by tuning the density of the polymeric material. The targets are prepared in copper washers of different thicknesses corresponding to the required foam target's thickness. The inner diameter of the washer is 3 mm. The material used is cellulose triacetate (TAC – $C_{12}H_{16}O_8$). The target structures are randomized 3D network of fibers for all these densities. However, the fibers size and separation (pore diameter) are altered with density. It is observed that with decrease in density from 50 mg/cc to 1 mg/cc, the average polymer fiber diameters decrease from 0.15 to 0.05 μm and their separation increase from 0.6 to 2.4 μm, however, the structure remains similar. Scanning Electron Microscope images of 3d structure of 2 mg/cc and 4 mg/cc TAC foams are shown in Fig. 1b. The mean density fluctuations are < 1% in the focal area Ø 300 μm. The low density TAC foams are developed using following steps. The cotton linters are mixed in glacial acetic acid for acetilation using acetic anhydride. This process is done in the presence of concentrated sulfuric acid acting as a catalyst. In order to dissolve this solution easily in hot chloroform and poorly in cold chloroform, the acetilation conditions are set in such a way to give maximum molecular-weight TAC with degree of substitution approximately 2.85-2.95. The strong transparent wet gel is formed by diluting the hot chloroform solvent of TAC with an equal amount of methanol placed in copper washer. The wet gel was cooled to 0°C by placing it in a supercritical CO_2 dryer. In this process, methanol exchanged with liquid CO_2 and transparent foam was obtained. The more details of the target development have been discussed elsewhere.[20]

The targets used in this experiment are of densities 2 mg/cc, 4 mg/cc, 7mg/cc, and 20 mg/cc with thicknesses 1030 µm, 520 µm, 280 µm and 100 µm respectively. The targets are therefore mass-matched such that the areal density (ρ.r) presented along the laser axis is held constant at around 0.2 mg/cm^2 since the thicknesses of the targets varies in inverse proportion to their densities. Two semiconductor x-ray diodes, each with a different filter are employed to monitor the x-ray emission from the targets. The filters employed are 5 µm nickel (5 - 8 keV) and 20 µm aluminum (4.5 - 16keV). The diodes are located 64 cm from the target, viewing the laser spot, at an angle of 45^0 from target normal.

The dynamic motion of the rear surface of the foam targets and plasma expansion are studied using transverse two-frame optical shadowgraphy. The magnification at the focal plane of the imaging lens is 3.5, spatial and temporal resolutions are 12 µm and 500 ps respectively. The details of the shadowgraphy system is reported somewhere else.[21]

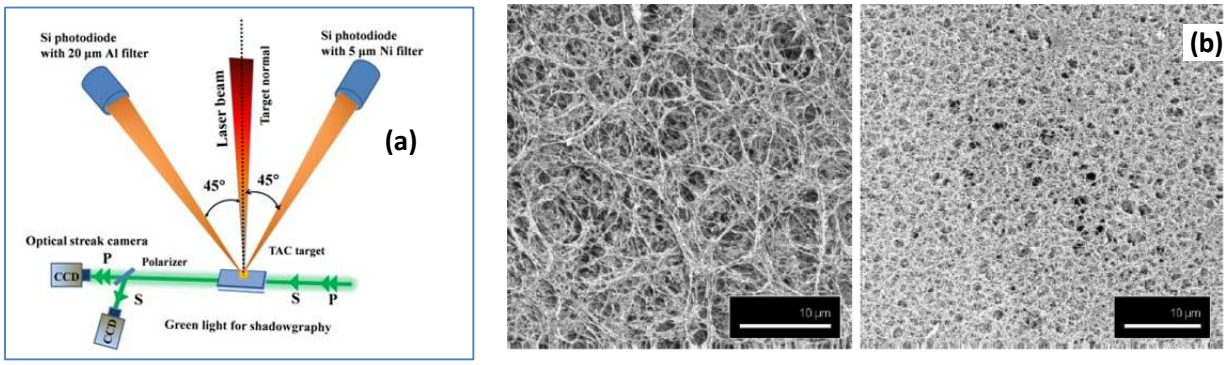

FIG. 1 (a) Schematic of various X-ray and ions diagnostics used in experiment. S and P are two second harmonic (532 nm) laser beams delayed by 3.5 ns to each other for the shadowgraphy of the target irradiated by laser (b) SEM record of 2 mg /cc and 4 mg/cc TAC foam target.

III. THEORETICAL SIMULATION

Simulations are performed using the Lagrangian one-dimensional radiation-hydrodynamics simulation code HYADES.[22] The simulations employ a flux-limited diffusion transport model for electron conduction and a multi-group diffusion model of radiation transport with 100 radiation groups, 99 of which are arranged logarithmically between 1 eV and 20 keV (the lower bound of the lowest energy group is set by default at 1 meV). A SESAME equation of state file is employed, however this file describes the equation of state of a continuous solid, rather than foam. In order to render the modelling more representative of the foam targets employed in the experiment, a foam model is employed in the simulation that amounts to having a variation in the density of material in the initial Lagrangian mesh from one cell to the next between some non-zero minimum (in this case 0.1 mg/cc) and twice the mean foam density such that the overall mean density of the target is preserved at the value employed in the experiment. An average atom model is employed in the in-line multigroup opacity calculation. While comparing with the experimental data, the effective surface area of the target of 1 cm^2 is taken into account in the simulation.

IV. RESULT AND DISCUSSION

The quantitative measurement of x-ray emission from the front surface of the mass-matched foam targets at constant laser energy of 7.5 J is performed using x-ray diodes in two spectral ranges, (5-8 keV) and (4.5 - 16 keV). The quantitative measurement of x-ray yield from the foam plasma was done by measuring the amount of charge generated by the x-ray photons of different spectral range using formula Q (charge created by photon) = V_{out} (voltage generated on oscilloscope) x C_F (capacitance used in pre-amplifier)[23]. Hence, the quantum efficiency (total number of electrons generated by x-ray photons) of the photodiodes were measured which is also

matching with the quantum efficiency data provided by manufacturers. The average energy required to generate 1 electron-hole pair is 3.6 eV. Once, we know the quantum efficiency and the number of electron-hole pairs generated, we can measure the energy of X-ray flux on the photodiodes. Finally, x-ray energy in μJ/ Sr obtained by dividing the total X-ray energy recorded by photo diode with the solid angle subtended by diode on target (on focal spot). Fig.2 and 3 show the hard x-ray yield variation with mass-matched targets in these spectral ranges. The x-ray yield (and hence the conversion efficiency) increases by a factor of 2.3 in the under-dense 2 mg/cc foam target as compared to over-dense 20 mg/cc target in both spectral ranges. The conversion efficiency for 2 mg/cc foam target increased by 137% compared to 20 mg /cc foam targets. Whilst there is an excellent match in the trend seen in the data between the simulation and the experiment, there is also some discrepancy between the absolute values. Given that the normalized data matches so well it is felt that this can be probably explained by the fact that the simulations are one-dimensional, and take no account of the intensity variation across the focal spot.

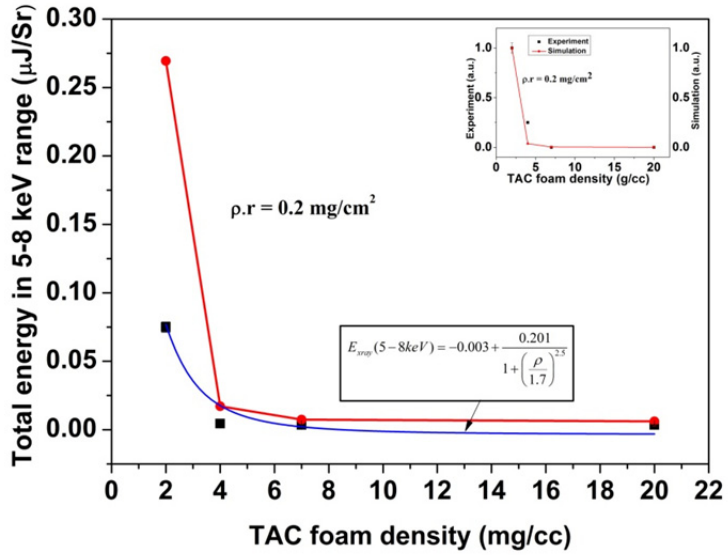

FIG. 2. Effect of foam density on soft x-ray emission in the spectral range 5 keV - 8 keV for a constant areal density of 0.2 mg/cm^2.

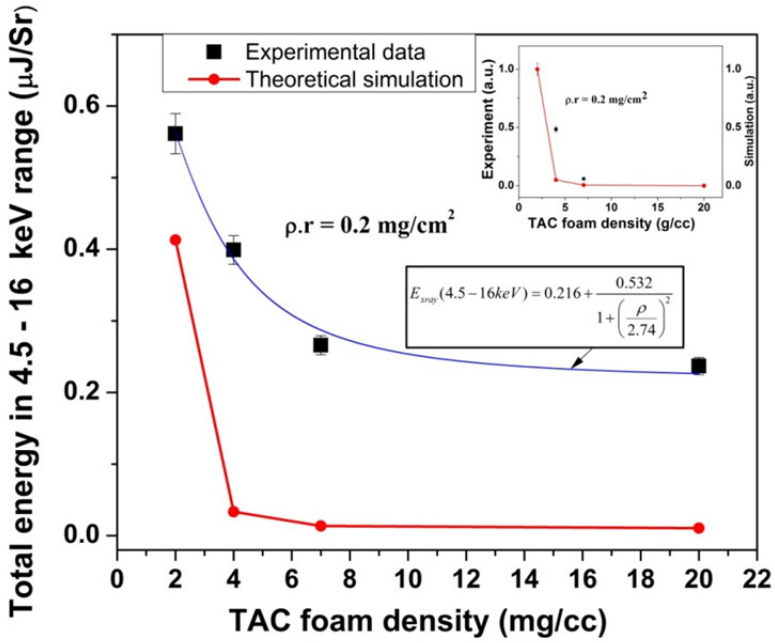

FIG. 3. Effect of foam density on soft x-ray emission in the spectral range (4.5 - 16 keV) for a constant areal density of 0.2 mg/cm^2.

The reason for the enhancement in the x-ray emission in lower density targets can be explained as follows. In under-dense material the heating is supersonic and volumetric. The enhancement of the volume of x-ray emission is due to initial penetration of laser to a large extent due to the transparency of target. This region is then converted into plasma of under critical density. However, in the case of over-dense material, the heat wave propagation is subsonic, taking the form of an ablation wave. In the case of under-dense (< 4mg/cc) plasma since the heating is supersonic, no hydrodynamic motion of the dense plasma takes place and hence no shock wave formation takes place. Therefore, there is no loss of energy in hydrodynamic motion. In the case of over- dense (> 4mg/cc) plasma, shock formation takes place which reduces the conversion of laser energy to x-ray energy. Yan Xu et al.,[24] has done simulations using the one-dimensional multi-group Radiation hydrodynamics code RDMG and shown that sub-critical density plasma is heated supersonically, and no shock wave formation takes place, while in over-dense plasma the situation is reversed. Our simulations demonstrated a similar effect, but, as previously mentioned, now with a "foam-like" initial density perturbation in the simulated plasma. The volumetric absorption phenomena can be further explained as follows. The dynamics of laser light absorption in low-density porous material is explained by a long homogeneous period during which there exist stochastically distributed sub-critical density regions in the plasma. As a result, the radiation is absorbed in a volume at the so called geometrical transparency length which is determined by classical collision mechanisms.[24]

$$L_T = \frac{9.2\times10^{-8}}{Z}\left(\frac{A}{Z}\right)^2 \frac{T^{3/2}}{\lambda^2.\rho^2} \qquad (1)$$

Here A and Z are the atomic number and charge of the plasma ions respectively, λ is the wavelength of the laser light (μm), T is the electron temperature (keV), and ρ is the plasma density (g/cm^3). From the above equation it is clear that the radiation absorption length is inversely proportional to the square of the density of the foam (plasma). Thus, the x-ray emitting volume of plasma in the case of a low-density target is higher and so the x-ray yield is enhanced. We have performed numerical fits to our experimental data as shown in Fig. 2 and 3. The x-ray yield varies with foam density in the two spectral ranges being investigated as follows:

$$E_{xray}(5-8keV) = -0.003 + \frac{0.201}{1+\left(\frac{\rho}{1.7}\right)^{2.5}} \quad \text{and} \quad E_{xray}(4.5-16keV) = 0.216 + \frac{0.532}{1+\left(\frac{\rho}{2.74}\right)^{2}} \qquad (2)$$

The scaling with density is similar to that predicted from theory as given by equation 1. The higher yield in the case of hard x-rays can also be explained by the fact that the supersonic heat-wave creates hot plasma which is denser and therefore more efficient in producing multi-keV x-rays. On the contrary, in an over-critical density targets, the formation of the ablation front results in material in the ablation front (subsonic heating in over-dense plasma) rising to a higher pressure. This results in a higher kinetic energy per unit of mass heated and a higher exhaust velocity than in a sub-critical density target. This is the reason for the enhancement of the coronal emission in the multi- keV x-ray region. To provide some information on the hydrodynamic behavior of the targets, we have set up a two-frame optical shadowgraph with time delay of 4.8 and 8.3 ns with respect to the arrival of the main laser pulse at the target. The shadowgraphs of 2 mg/cc and 20 mg/cc foam targets at three time delays i.e., t = 0 ns, t = 4.8 ns, and 8.4 ns are shown in the Fig. 4a-f. From the figure, it is seen that the plasma diameter and the rear surface accelerated targets exceeds the laser focal spot size (100 μm) on the 2 mg/cc foam

target by several times. The diameter of laser produced plasma reaches approx 1494 μm at a delay of 8.3 ns due to fast lateral heat transport in the low-density target and reduces to approximately half of this for the 20 mg/cc density target. This enhanced lateral dimension of plasma and rear surface accelerated foam target may be due to the larger volume heating in case of low-density foam (2 mg/cc). However, it is lower and more directional for 20 mg/cc (supercritical) foam targets which may be due to shock wave and subsonic directional heating.

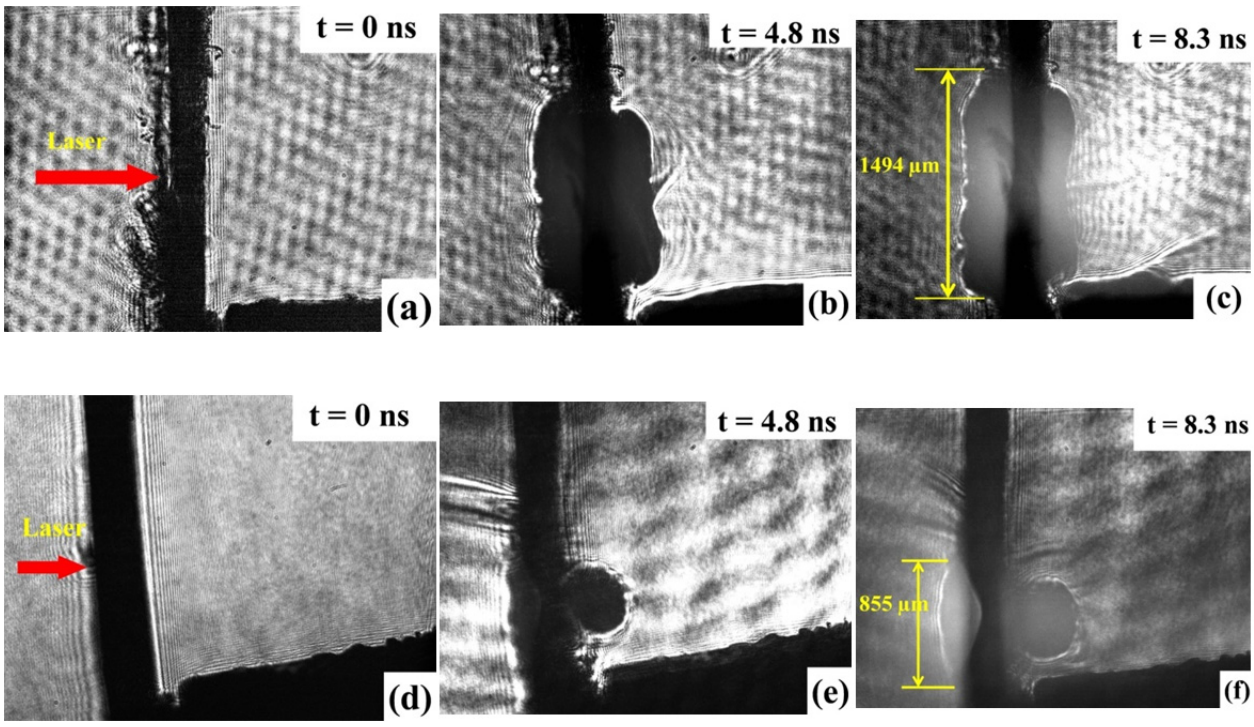

FIG. 4. Shadowgraph of 2 mg/cc foam target at a delay of (a) t = 0 ns, (b) t = 4.8 ns, (c) t = 8.3 ns relative to the arrival of the laser pulse, and for the 20 mg/cc foam targets at delays of (d) t = 0 ns, (e) t = 4.8 ns, and (f) t = 8 ns.

V. CONCLUSION

The x-ray emission from mass-matched low-density triacetate cellulose (TAC) foam targets with densities in the range 2 mg/cc to 20 mg/cc irradiated by an Nd:Glass laser at ~ 2 x 10^{14} W/cm^2 in an approximately 500 ps pulse is reported. The x-ray emission is measured in two spectral ranges, (5 - 8 keV) and (4.5- 16 keV). It is found that the emission is approximately 2.3 times greater in 2 mg/cc foam targets as compared to 20 mg/cc foam targets. Simulations are performed using a one-dimensional radiation-hydrodynamics code to verify the experimental results. The simulations agree well with the experimental results.

ACKNOWLEDGEMENTS

The authors from BARC wish to acknowledge the support and continuous encouragement received from Dr. S. M. Sharma, former Director, Physics group and Dr. N. K. Sahoo, Associate Director, Physics Group, BARC. Also, we acknowledge the excellent support given by Mr C. G. Murali, Mrs P. Leshma, Mr. D. S. Munda and Mr Ritesh Sabale in the design and implementation of the laser electronics and in the smooth operation of the laser system. Authors acknowledge the financial support received by Department of Science & Technology (DST) under DST-RFBR project (INT/RUS/RFBR/P-218).

[1.] J. D. Lindl, P. Amendt, R. L. Berger, S. G. Glendinning, S. H. Glenzer, S.W. Haan, R. L. Kauffman, O. L. Landen, and L. J. Suter, Phys. Plasmas **11**, 339 (2004).

[2.] J. Denavit and D. W. Phillion, Phys. Plasmas **1**, 1971 (1994).

[3.] J. A. Koch, K. G. Estabrook, J. D. Bauer, C. A. Back, L. Klein, A. M. Rubenchik, E. J. Hsieh, R. C. Cook, B. J. MacGowan, J. D. Moody, J. C. Moreno, D. Kalantar, and R. W. Lee, Phys. Plasmas **2**, 3820 (1995).

[4] C. Constantin, C. A. Back, K. B. Fournier, G. Gregori, O. L. Landen, S. H. Glenzer, E. L. Dewald and M. C. Miller, Phys. Plasmas **12**, 063104 (2005).

[5] K. B. Fournier, M. Tobin, J. F. Poco, K. Bradley, C. A. Coverdale, D. Beutler, T. Vidnovic, M. Severson, E.A. Smith, D.L. Reeder, 332nd EPS Conference on Plasma Phys. Tarragona, 27 June - 1 July 2005 ECA Vol.29C, P-1.145 (2005).

[6] F. Girard, J. P. Jadaud, M. Naudy, B. Villette, D. Babonneau, M. Primout, M. C. Miller, R. L. Kauffman, L. J. Suter, J. Grun, and J. Davis, Phys. Plasmas **12**, 092705 (2005).

[7] O. Willi, L. Barringer, C. Vickers and D. Hoarty, The Astrophysical Journal Supplement Series **127**, 527 (2000).

[8] L. J. Suter, R. L. Kauffman, M. S. Maxon, J. F. Davis, UCRL-JC-123590 (1996).

[9] K. B. Fournier, C. Constantin, J. Poca, M. C. Miller, C. A. Back, L. J. Suter, J. Satcher, J. Davis, and J. Grun, Phys. Rev. Lett. **92**, 165005 (2004).

[10] S. Chaurasia, S. Tripathi, D. S. Munda, G. Mishra, C. G. Murali, N. K. Gupta, L. J. Dhareshwar, A. K. Rossall, G. J. Tallents, R. Singh, D. K. Kohli, and R. K. KhardekarPramana, J. Phys. **75**, 1191 (2010).

[11] S. Yu. Guskov, Laser Part. Beams **23**, 255 (2005).

[12] S. Yu. Guskov, A.I. Gromov, Yu. A. Merkulev, V.B. Rozanov, V.V. Nikishin, V.F. Tishkin, N.V. Zmitrenko, V.V. Gavrilov, A.A. Goltsov, V.N. Kondrashov, N.V. Kovalsky, M.I. Pergament, S.G. Garanin, G.A. Kirillov, S.A. Sukharev, A. Caruso and C. Strangio, Laser Part. Beams **18**, 1 (2000).

[13] S. W. Haan, S. M. Pollaine, J. D. Lindl, L. J. Suter, R. L. Berger, L. V, Powers, W. E. Alley, P. A. Amendt, J. A. Futterman, W. K. Levedahl, M. D. Rosen, D. P. Rowley, R. A. Sacks, A. I. Shestakov, G. L. Strobel, M. Tabak, S. V. Weber, G. B. Zimmerman, W. J. Krauser, D. C.

Wilson, S. V. Coggeshall, D. B. Harris, N. M. Hoffman, and B. H. Wilde, Phys. Plasmas **2**, 2480 (1995).

[14.] W. J. Krauser, N. M. Hoffman, D. C. Wilson, B. H. Wilde, W. S. Varnum, D. B. Harris, F. J. Swenson, P. A. Bradley, S. W. Haan, S. M. Pollaine, A. S. Wan, J. C. Moreno, and P. A. Amendt, Phys. Plasmas **3**, 2084 (1996).

[15.] T. Hall, D. Batani, W. Nazarova, M. Koenig, A.Benuzzi, Laser Part. Beams **20**, 303 (2002).

[16.] R. Benocci, D. Batani, R. Dezulian, R. Redaelli, G. Lucchini, F. Canova, H. Stabile, J. Faure, E. Krousky, K. Masek, M. Pfeifer, J. Skala, R. Dudzak, M. Koenig, V. Tikhonchuk, Ph. Nicolaý¨, and V. Malka, Phys. Plasmas. **16**, 012703 (2009).

[17.] Y. Xu, J. Zhang, J. Yang, W. Pei, Y. Ding, D. Lai, G. Men, and Z. Luo, Phys. Plasmas **14**, 052701 (2007).

[18.] J. Limpouch, N. N. Demchenko, S. Yu. Gus'kov, M. Ka´lal, A. Kasperczuk, V. N. Kondrashov, E. Krousky, K. Macek, P. Pisarczyk, T. Pisarczyk, and V. B. Rozanov, Plasma Phys. Controlled Fusion **46**, 1831(2004).

[19.] D. Batani, A. Balducci, W. Nazarov, T. Lower, T. Hall, M. Koenig, B. Faral, A. Benuzzi, M. Temporal, Physical Review E **63**, 046410 (2001).

[20.] N. G. Borisenko, I. V. Akimova, A. I. Gromov, A. M. Khalenkov, Yu. A. Merkuliev, V. N. Kondrashov, J. Limpouch, J. Kuba, E. Krousky, K. Masek, W. Nazarov, V. G. Pimenov, Fusion Science and Technology **49**, 676 (2006).

[21.] S. Chaurasia, P. Leshma, S. Tripathi, C. G. Murali, D. S. Munda, N. K. Gupta, L. J. Dhareshwar, S. M. Sharma, S. Kailas, BARC News Letter, Issue **317**, 13 (2010).

[22.] HYADES is a commercial product of Cascade Applied Sciences. Email: larsen@casinc.com

[23.] S. Chaurasia, D. S. Munda, L. J. Dhareshwar, BARC Report BARC/2008/E/19 (2008).

[24.] Yan Xu, Tuo Zhu, Shuanggui Li, and J. Yang, Phys. Plasmas **18**, 053301 (2011).

[25.] A. E. Bugrov, S. Yu. Guskov, V. B. Rozanov, I. N. Burdonskii, V. V. Gavrilo, A. Yu. Goltsov, E. V. Zhuzhukalo, N. G. Kovalskii, M. I. Pergament and V. M. Petryakov, JETP **84 (3)**, 497 (1997).